Austin Journal of Analytical & Pharmaceutical Chemistry

Open Access

Austin Publishing Group

Research Article

Aptamer Functionalised Small Gold Nanorod-Based Nanoprobes: Targeting EpCAM Over-expressed Cancer Cells for Photothermal Therapy

Mbalaha ZS[1,2]; Craig G[1,3]; Birch DJS[1]; Chen Y[1*]

[1]Department of Physics, Scottish Universities Physics Alliance, University of Strathclyde, 107 Rottenrow, Glasgow G4 0NG, UK

[2]Joseph Sarwuan Tarka University, Makurdi, P.M.B. 2373, Makurdi, Benue state, Nigeria

[3]Tayside Clinical Trials Unit, Tayside Medical Science Centre, Ninewells Hospital & Medical School, University of Dundee, George Pirie Way, Dundee, DD1 9SY, UK

***Corresponding author: Chen Y**

Department of Physics, Scottish Universities Physics Alliance, University of Strathclyde, 107 Rottenrow, Glasgow G4 0NG, UK.

Tel: +44 (0)141 548 3087

Email: y.chen@strath.ac.uk

Received: April 10, 2024

Accepted: May 08, 2024

Published: May 15, 2024

Abstract

Small Gold Nanorods (SGNRs) are beneficial for photothermal therapy owing to their exceptional properties such as high binding and internalization rate into cells, as well as efficient heat generation. We have functionalized small gold nanorods with SYL3C aptamer to target EpCAM-expressed cancer cells. A higher binding rate was observed in cancer cells with over-expressed EpCAM (PC3, FLO-1 and MCF-7) than the non-tumour cells (HEK293), indicating specific binding of the nanoprobes. Z-stack fluorescence microscopy analysis revealed that the nanoprobes bind to the cell membrane of FLO-1 and MCF-7 cancer cells. It was found that SYL3C nanoprobes of different sizes introduced more death in FLO-1 cells than in HEK293 cells and the death rate of FLO-1 treated with small gold nanorod-based SYL3C nanoprobe was significantly higher than that treated with large gold nanorod-based nanoprobes. These findings demonstrate an enhanced efficacy of aptamer functionalized small gold nanorods in photothermal therapy resulting from an increased affinity to EpCAM expressed cancer cells and the enhanced photothermal effect of the small gold nanorods, thus providing insight into the development of gold nanoprobes for efficient photothermal therapy of cancer.

Keywords: Gold nanorods; Epithelia cell adhesion molecule (EpCAM); SYL3C; Photothermal therapy; Aptamer

Introduction

In the field of photothermal therapy, the use of contrast agents with high heat conversion efficiency and targeting capabilities is desirable for enhancing treatment efficacy while minimizing side effects. Gold Nanorods (GNRs) have emerged as a good candidate because of their surface plasmon enhanced photothermal effect and shape dependent tunable optical properties [1-5]. Especially Small Gold Nanorods (SGNRs) functionalized with targeting agents of high binding affinity and specificity for cancerous cells provide a promising solution [6,7]. Compared to Large Gold Nanorods (LGNRs), which exhibit a length and width greater than 40 nm and 10 nm, respectively, the SGNRs with a length of less than 20 nm and a width of less than 10 nm exhibit larger binding and internalization rates, higher absorption-to-extinction ratio and greater heat generation [8,9]. In addition, the photothermal effect of SGNRs is less sensitive to the excitation wavelength and can generate a high temperature rise even at off-resonance excitation, thus more beneficial than LGNRs for photothermal applications in biological systems [10]. These advantages, along with biocompatibility, deep tissue penetration, photostability and large surface area-to-volume ratio [11,12], make SGNRs ideal for targeting receptors, delivering therapeutic drugs, and photothermal therapy [13,14]. Gold nanorods have shown potential in the photothermal therapy of cancer because of their enhanced heat generation capabilities. Recent studies have demonstrated that GNRs kill cancer cells [15,16] For example, Vu et al demonstrated that a GNR based nanocomposite destroyed 70% of OML-1oral cancer cells under photoexcitation [17]. Doxorubicin loaded GNR under laser excitation were found to simultaneously enhance drug release and induce 93% of $HepG_2$ cell necrosis [18]. The size of GNRs influence their photothermal effect [10,13]. We have demonstrated recently that the SGNRs have higher photothermal effect than the LGNRs in a mimic extracellular environment [10]. In addition, it has been reported that SGNRs showed much higher macrophage uptake and negligible cytotoxicity in comparison with LGNRs to form healthy BSA-coated SGNR-laden-macrophages that exhibited significantly improved photothermal conversion in the tumour [19]. Targeting of cancer cells could be challenging due to the heterogeneity of extracellular matrix. Gold nanorods functionalized with targeting ligands have shown higher cellular uptake and specificity for cancerous cells, suggesting that such targeting ligands could reduce the

Citation: Mbalaha ZS, Craig G, Birch DJS, Chen Y. Aptamer Functionalised Small Gold Nanorod-Based Nanoprobes: Targeting EpCAM Over-expressed Cancer Cells for Photothermal Therapy. Austin J Anal Pharm Chem. 2024; 11(1): 1170.

adverse effects on healthy cells [20]. It was found that integrin-targeting gold nanoparticles assisted plasmonic photothermal therapy caused a cancer cell motility decrement resulting from cytoskeletion transformation and inhibit metastasis [21]. Pitsillides et al have reported effective thermal-induced activation of cell death using anti-CD-8-labeled gold nanoparticles for selective targeting [21]. Despite their potential, research in developing nanoprobes based on functionalized SGNRs with targeting ligands such as aptamer has been limited.

Aptamers, are synthetic single-stranded biological molecules created through Systematic Evolution of Ligands by Exponential enrichment (SELEX) from either a DNA or RNA. Aptamers bind to a variety of targets including proteins, nucleic acids and metal ions and have been utilized to transport therapeutic agents, target RNAs and proteins, detect disease biomarkers and contaminants in food [22-26]. Aptamers are non-immunogenic, non-toxic, and have small sizes (1.2 nm-3 nm) for effective binding and deep tissue penetration. DNA aptamers are preferred in most clinical applications due to their stability and resistance to nuclease degradation [27]. The SYL3C aptamer, is a dual-loop hairpin DNA, that binds to epithelia cell adhesion molecule (EpCAM) expressed on the cell membrane of cells of epithelia origin [23-26]. EpCAM over-expression is common in prostate cancer, breast cancer, colorectal cancer and oesophagus cancer [23,28-31]. SYL3C aptamer has been found to bind to EpCAM over-expressed cancer cells with high affinity and specificity but not to non-EpCAM over-expressed cells [29]. Gold nanoparticles functionalized with SYL3C have shown high efficiency and specificity in capturing circulating tumour cells with high levels of EpCAM over-expression [32,33]. SYL3C aptamer staining was found to detect 98% EpCAM over-expression in both oesophagus squamous cell carcinoma and oesophagus adenocarcinoma, but not in normal oesophagus epithelium[34].

Herein, we reported for the first time the SYL3C aptamer functionalized small gold nanorods to target EpCAM over-expressed cancer cells for photothermal therapy. This study investigated the efficacy of SYL3C-functionalized SGNRs in targeting EpCAM-overexpressed cancer cells and the impact of size on their photothermal efficiency. The findings provide important insight into the development of small gold nanorod-based nanoprobes for improved photothermal therapy.

Experimental Section

Materials

All chemicals were used as received without further purification. Chloroauric acid ($HAuCl_4$, 49%), Hexadecyltrimethylammonium Bromide (CTAB, 99%), Ascorbic Acid (AA), Sodium borohydride ($NaBH_4$, 99.8%), Silver nitrate ($AgNO_3$), Dodecanethiol (DDT, 98%), Mercaptohexanoic Acid (MHA, 99.8%), Acetone (99.9%), Isopropanol (99.5%), Toluene (99.8%) and methanol were purchased from Sigma Aldrich while Hydrochloric Acid (HCL) was purchased from Fluka.

The SYL3C aptamer and the cDNA were purchased from Sigma Aldrich. To confirm the successful functionalization of the aptamer, SYL3C was labelled with Cy3.

Table 1: The dimensions and LSPR of the $SGNR_1$, $SGNR_2$ and the LGNR.

Samples	LSPR (nm)	Length (nm)	Width (nm)
$SGNR_1$	789	22.0±4.6	5.8±1.3
$SGNR_2$	679	18.5±4.2	5.4±1.4
LGNR	760	45.0±7.2	11.6±2.0

Cy3-SYL3C aptamer:

5'[ThiC6]AAAAAACACTACAGAGGTTGCGTCTGTCCCACGTTGTCATGGGGGGTTGGCCTG[Cy3]-3',

cDNA:

5'-CAGGCCAACCCCCCATGACAACGTGGGACAGACAGACGCAACCTCTGTAGTG-3'.

Synthesis of Gold Nanorods

Large gold nanorods were synthesized using a reported protocol [35]. Two samples of the small gold nanorods ($SGNR_1$ and $SGNR_2$) were synthesized using our modified silver assisted seed-mediated growth method [36]. Briefly, the seed solution was prepared by adding $HAuCl_4$ to a solution of CTAB. Thereafter, a freshly prepared ice-cold $NaBH_4$ solution was added to the mixture and stirred with a magnetic stirrer for 2-3 min until the seed solution turned a dark brown color. The solution was incubated at room temperature for 2hr for gold seeds growth before use. To prepare the growth solutions, $HAuCl_4$, $AgNO_3$ and HCL were added to CTAB solution. After thorough mixing, AA was added. Finally, the seed solution was added to the growth solution. Table S1 and S2 list all the reagents used for the preparation of LGNR, $SGNR_1$ and $SGNR_2$.

Ligand Exchange and Functionalization of Gold Nanorods

Ligand exchange and functionalization of gold nanorods were performed using protocols described in our previous works [35,36]. Briefly, CTAB on as made gold nanorods was replace with MHA using a round trip ligand exchange processes. The pellets of ligand-exchanged gold nanorods were suspended in TBE buffer. Following the ligand exchange, the gold nanorods were functionalized with thiolated SYL3C aptamer via a salting process according to a previous protocol [35-37]. The thiolated aptamer was activated with tris (2-carboxyethyl) phosphine hydrochloride (TCEP, 10 µl). The aptamer was conjugated with gold nanorods in a molar ration of 400:1 using a previously reported salt aging procedure [35-37]. The conjugates were washed at 4°C and resuspended in phosphate buffer after centrifuging.

Cell Sample Preparation

Prostate cancer cell line, PC3, as EpCAM positive cell, and a non-tumour human kidney cell line, HEK293, as EpCAM negative cell were used to evaluate the specificity of the small gold nanorod based SYL3C aptamer nanoprobe. Both PC3 and HEK293 cell lines were seeded at 1.5 x 10^6 cells per well in a 6-well plate in a Dulbecco's Modified Eagle's Medium (DMEM) media containing FBS (10%) and penicillin-streptomycin (5.5ml). Both PC3 and HEK293 cells were incubated with 0.1 nM $SGNR_2$-SYL3C nanoprobes or $SGNR_2$-MHA for 4 hours in separate wells. Following the incubation, the cells were centrifuged at 1400 rpm for 5 minutes and re-suspended in PBS buffer for flow cytometry. Furthermore, human esophagus adenocarcinoma cell line, FLO-1 and breast cancer cell line, MCF-7 were chosen to investigate the time dependent uptake and binding site of SYL3C aptamer functionalized small gold nanorods on other cancer cells of epithelia origin. FLO-1 and MCF-7 cancel cell lines with similar cell density as above were cultured on coverslips suspended in the DMEM media in 24 well plate overnight after which the cells were treated with $SGNR_2$-SYL3C nanoprobes and $SGNR_2$-MHA for 0.5 hours, 1 hour and 1.5 hours respectively. After the incubation, the FLO-1 and MCF-7 cell samples were further treated with 4, 6-Diamidine-2-phenylindole (DAPI) to stain the cell nuclei.

Biocompatibility Study of $SGNR_1$-SYL3C Nanoprobe

The biocompatibility of SYL3C based nanoprobes was evaluated by incubating the $SGNR_1$-SYL3C nanoprobe with FLO-1, MCF-7 and HEK293 cell lines in comparison with the $SGNR_1$-MHA. Specifically, 8.0 x 10^5 cells of each cell line seeded in 2 ml of the DMEM medium were incubated with 0.4 nM of the $SGNR_1$-SYL3C nanoprobe and the $SGNR_1$-MHA for 3 hours. Thereafter, the cells were washed with PBS, tyrpsinized, centrifuged and re-incubated in 1 ml of the fresh DMEM medium for 24 hours to assess cell viability.

Sample Preparation and Photothermal Effect Study

FLO-1 and the HEK293 cell lines were cultured in the DMEM media and incubated with the 0.4 nM of $SGNR_1$-SYL3C, $SGNR_1$-MHA, LGNR-SYL3C, and LGNR-MHA for 1.5 hours. Thereafter, the cells were washed with PBS and re-suspended in 300 µl of red phenol free DMEM medium for photo-excitation. Then, 20 µl of the treated cell samples and un-treated cells were placed on an improvised chamber made from the lid of a 1.5 ml Eppendorf tube for excitation.

The cell samples treated with the SGNR- SYL3C and SGNR-MHA were excited on resonance to the surface plasmons resonance of the $SGNR_1$ (774 nm with laser power density 0.346±0.060W/cm^2) for enhanced heat generation for 1 min. On the other hand, the cell samples treated with the LGNR nanoprobe, LGNR-MHA and the control cell samples were excited on resonance to the surface plasmon resonance of LGNR (753 nm with laser power density 0.306±0.050W/cm^2) for 1 min. After laser exposure, 10 µl of the laser treated cell samples were mixed with 5 µl trypan blue (0.4%) on a glass slide to identify viable and dead cells. The trypan blue treated cell samples were imaged with a confocal microscope using the 10x objective lens. The quantities of viable and dead cells were determined by casting the entire laser treated cells mixed with trypan blue on a hemocytometer for counting. Cell necrosis was determined according to equation 1.

$$\text{Cell Necrosis } (\%) = \frac{\text{Total number of dead cells}}{\text{Total number of counted cells}} \text{ x } 100 \quad (1)$$

where the total number of counted cells is the sum of live and dead cells from the photoexcited cell lines. Standard deviation was calculated from the four replicas.

Optical Characterization of Gold Nanoprobes

The extinction spectra of the $SGNR_1$, $SGNR_2$ and LGNR samples were measured with a UV-visible spectrophotometer (Lambda 2, Perkin Elmer).

Flow cytometry analysis was performed using a A MoFlo XDP cytometer (Beckman Coulter, Brea, CA) at 532 nm excitation. Fluorescence imaging was performed using a confocal microscope (Leica Microsystems SP8). The samples were excited at 405 nm for DAPI and 561 nm for Cy3.

Results and Discussion

Synthesis of SYL3C Functionalized Gold Nanorods

Gold nanorods ($SGNR_1$, $SGNR_2$ and LGNR) were synthesized with Longitudinal Surface Plasmon Resonance (LSPR) at 789 nm, 679 nm and 760 nm respectively. The average dimensions of these GNRs were determined from SEM images and listed in table 1 together with their LSPR.

Figure 1 shows the UV-vis extinction spectra of the $SGNR_1$, $SGNR_2$ and the LGNR before, after ligand exchange (GNR-MHA) and functionalization with the SYL3C (GNR-SYL3C) respectively. The longitudinal surface plasmon resonance of $SGNR_1$, $SGNR_2$ and LGNR was centered at 756 nm, 676 nm and 765 nm respectively without apparent peak broadening after the ligand exchange. After functionalization with the SYL3C, the LSPR of $SGNR_1$-SYL3C, $SGNR_2$-SYL3C and the LGNR-SYL3C nanoprobes were centered at 774 nm, 634 nm and 753 nm. $SGNR_2$-SYL3C was used in binding studies because fluorescence is enhanced when LSPR is close to the emission of Cy3. On the other hand, $SGNR_1$-SYL3C was used in phototherapy studies as its LSPR matches the biological window.

Furthermore, $SGNR_1$-SYL3C, $SGNR_2$-SYL3C and LGNR-SYL3C nanoprobes were incubated with cDNA in the ratio 1:1000 and their UV-vis extinction spectra are presented in Figure 1c, d, e & f. The peak centered at ~259 nm representing the absorption of DNA (SYL3C). Figure 2 shows the fluorescence emission spectra of the $SGNR_1$-SYL3C, $SGNR_2$-SYL3C and the LGNR-SYL3C nano-

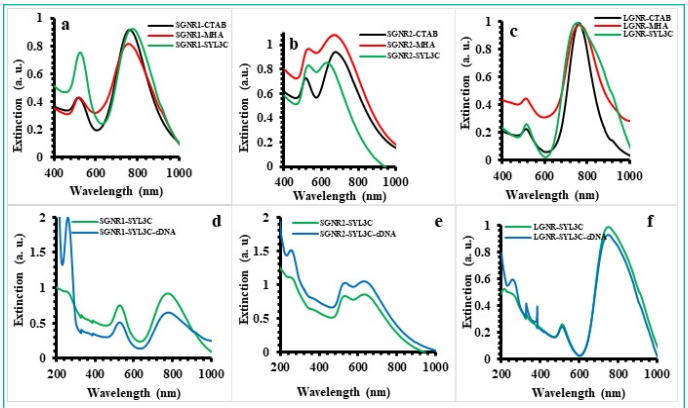

Figure 1: The UV-vis extinction spectra of (a) SGNR1, (b) SGNR2 and (c) LGNR before/after ligand exchange and functionalization with SYL3C, of (d) SGNR1-SYL3C, (e) SGNR2- SYL3C and (f) LGNR-SYL3C nanoprobes incubated cDNA.

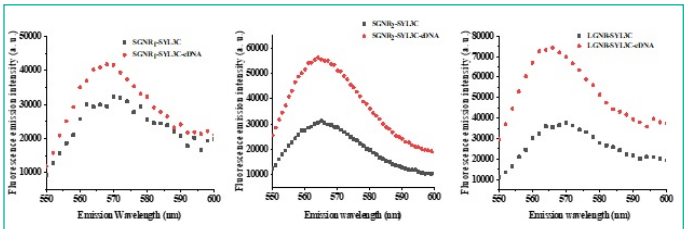

Figure 2. The fluorescence emission spectra of Cy3 in the gold nanorods nanoprobes before and after hybridization; (a) $SGNR_1$-SYL3C nanoprobe, (b) $SGNR_2$-SYL3C nanoprobe (c) LGNR-SYL3C nanoprobe.

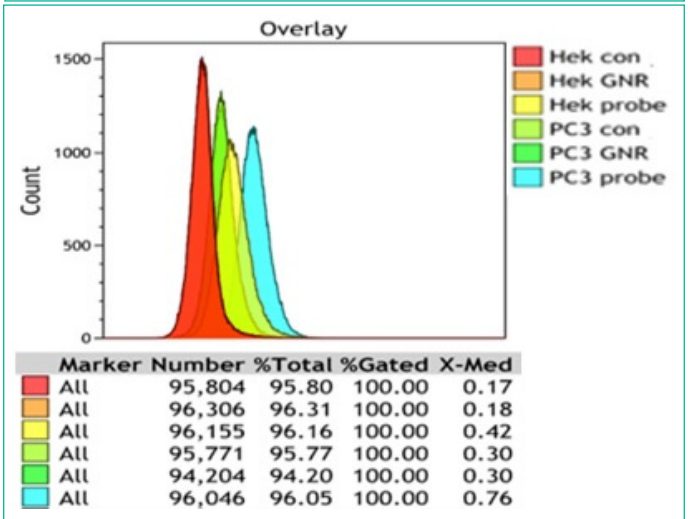

Figure 3: The histogram of the distribution of fluorescent intensity for different cell lines.

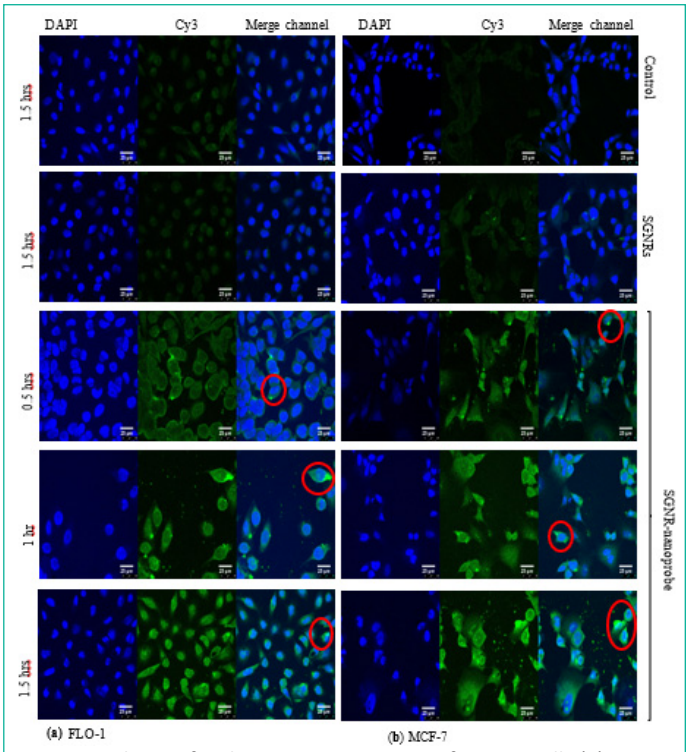

Figure 4: The confocal microscopic images of cancer cells (a) FLO-1 and (b) MCF-7 treated with $SGNR_2$-SYL3C nanoprobes for 0.5 hours, 1 hour and 1.5 hours in comparison to the control cells and the cells treated with $SGNR_2$-MHA for 1.5 hours.

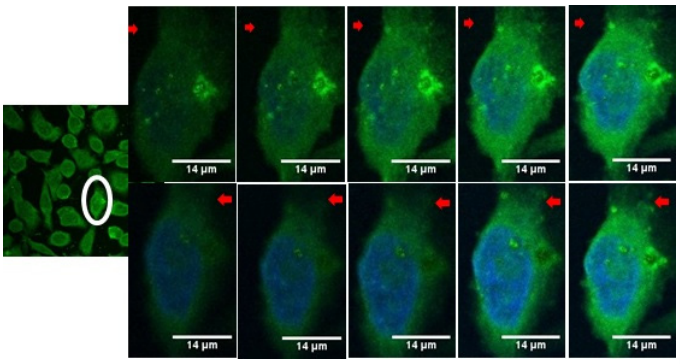

Figure 5: The Z-stack of the SGNR2-SYL3C nanoprobe incubated with FLO-1 cells 1.5 hours.

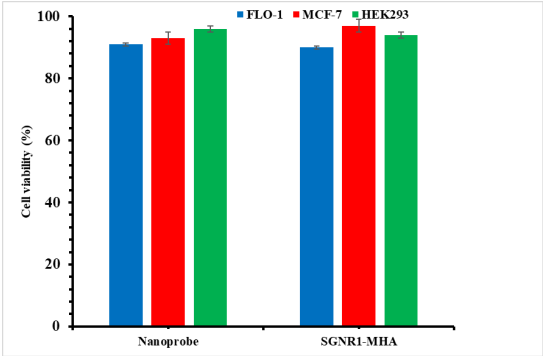

Figure 6: The biocompatibility of $SGNR_1$-SYL3C aptamer nanoprobe.

probes before and after incubating with the cDNA at 532 nm excitation. The increase of the fluorescence emission intensity of Cy3 nanoprobes after adding cDNA was observed in all three cases.

In the absence of cDNA, the aptamer was in a closed form where Cy3 at the end of SYL3C (donor) is close to the gold nanorod (acceptor) surface, resulting in quenching of Cy3' emission due to energy transferred from the donor to the acceptor. In the presence of the cDNA, the hybridization of cDNA with the aptamer transformed the aptamer into an opened configuration and shifted the fluorophore away from the gold surface, resulting in a recovered fluorescence emission. The increase in the fluorescence emission intensity of the $SGNR_1$-SYL3C, $SGNR_2$-SYL3C and the LGNR-SYL3C nanoprobes after hybridization with the cDNA confirms the successful functionalization of both the small and large gold nanorods with the aptamer.

Targeting EpCAM Expressed Cancer Cells with SGNR-SYL3C Nanoprobes

To confirm the specific targeting of SYL3C functionalized GNRs to EpCAM-expressing cancer cells, flow cytometry was employed and the cell binding of the nanoprobes were compared between EpCAM-positive and control cell lines. Recently, Zhong et al have shown that gold-magnetic nanoparticles functionalized with Eppc6 and Eppc14 aptamers were able to discriminate prostate cancer cell lines (PC3, DU145 and LNCaP) with over-expression of EpCAM from a normal kidney cell line HEK293 with low EpCAM expression [38]. Here, PC3 and HEK293 cell lines were used as EpCAM positive and negative cells in flow cytometry study to assess the targeting specificity of SGNR-SYL3C nanoprobes.

Figure 3. shows the cell population against Cy3 fluorescent intensity from PC3 and HEK293 cells treated with $SGNR_2$-SYL3C and $SGNR_2$–MHA, as well as two cell controls. HEK293 control and HEK293 with $SGNR_2$–MHA show autofluorescence of median 0.17 and 0.18, while PC3 control and PC3 with $SGNR_2$–MHA show a median of 0.3. The autofluorescence of PC3 cells is larger than that of HEK293. Fluorescence intensity of HEK293 and PC3 cells treated with $SGNR_2$ -SYL3C were found to be 0.42 and 0.76. The increase in the fluorescence intensity arises from Cy3 in the $SGNR_2$–SYL3C nanoprobes indicating the uptake of nanoprobes. Notably, the increase observed from PC3 is 1.83 times larger than that from HEK293 (0.46:0.25). The near-double increment in fluorescence intensities of nanoprobe treated PC3 against the nanoprobe treated HEK293 demonstrates a higher amount of $SGNR_2$-SYL3C nanoprobes bound to the PC3 cells. This is consistent with the high expression of EpCAM in the PC3 cell line, while the HEK293 cell line is a non-tumorous kidney cell with low EpCAM expression [37,39-42], confirming the specificity of the $SGNR_2$-SYL3C nanoprobe to recognize EpCAM on cancer cells.

To further understand the uptake dynamics of the $SGNR_2$-SYL3C nanoprobe by the EpCAM over-expressed cancer cells, cellular imaging was performed on the nanoprobe treated cancer cells, namely MCF-7 and FLO-1, in comparison with the two controls (cell only and cell treated with $SGNR_2$-MHA). MCF-7 and FLO-1 were chosen as they are EpCAM positive cell lines as PC3 and implication of $SGNR_2$-SYL3C nanoprobes in photothermal therapy of breast cancer and esophagus cancer. Figure 4 shows the fluorescent microscopic images of the cell control (un-treated), $SGNR_2$-MHA treated cells and the nanoprobe treated cells. The nucleus of the cells was stained by DAPI (blue) while nanoprobes were labeled with Cy3 (green). It can be seen that the cells treated with the $SGNR_2$-SYL3C nanoprobe display strong fluorescence signals in the Cy3 channel in contrast with the weak background from autofluroescence observed in the control group and the small gold nanorods treated cells, indicating the binding of the nanoprobe to the EpCAM expressed cancer cells. Figure 4 shows that at 0.5 hours, a few bright spots correlated to the nanoprobes attached to the cancer cells as highlighted by the red circles. With the increase of incubation time, more bright spots were found on the cells after incubation

for 1 hour and 1.5 hours. The increase of bright areas observed at longer incubation time suggests more nanoprobes attached to the cancer cells. These confirm that $SGNR_2$-SYL3C nanoprobes bind to various cancer cells with high EpCAM expression and more $SGNR_2$-SYL3C nanoprobes binds to the EpCAM over-expressed cancer cells at longer incubation time.

Furthermore, Z-stack analysis was performed to reveal the location of the attached nanoprobes on the cancer cell. Figure 5 depicts the Z-stack images of FLO-1 cancer cells treated with nanoprobes for 1.5 hours. The z-plane scanning as indicated by the trajectory of the red arrows reveals that the nanoprobes are mostly located on the cell membrane as expected because the receptor (EpCAM) resides on the cell membrane.

It is clear that $SGNR_2$-SYL3C nanoprobes exihibit a strong binding affinity to EpCAM positive cells (PC3, FLO-1, MCF-7). This targeting specificity is attributed to the high affinity of SYL3C apatermar to EpCAM present on the cell membrane. This specificity is evident in the clear distinction between $SGNR_2$-SYL3C nanoprobes targeting EpCAM positive and negative cell lines, as well as the discrimination between SYL3C functionalised gold nanorods ($SGNR_2$-SYL3C nanoprobes) and non-SYL3C gold nanorods ($SGNR_2$–MHA) in their binding to EpCAM positive cells. It is important to note that both $SGNR_2$-SYL3C nanoprobes and $SGNR_1$-SYL3C nanoprobes have strong affinity to cells expressing high levels of EpCAM due to SYL3C functionalization. Additionally, the slight difference in aspect ratio of the gold cores (3.4 vs. 3.8) doesn't significantly affect cell uptake, especially so when considering that most nanoprobes remain on the cell membrane after 1.5 hrs, as observed in Figure 5.

Biocompatibility of Small Gold Nanorods Aptamer Nanoprobe

Cell viability was investigated to evaluate the biocompatibility of the $SGNR_1$-SYL3C nanoprobe to FLO-1, MCF-7 and HEK293 cells after incubation for 24 hours. The total cells (viable and dead cells) were counted and the percentage of viable cells was determined. Figure 6 displays the bar chart representing the percentage of the viable cells after incubation with the $SGNR_1$-SYL3C nanoprobe and $SGNR_1$ – MHA. The cytotoxicity of the $SGNR_1$-SYL3C nanoprobe was found to be very small and similar to that of $SGNR_1$ – MHA. It can be seen that >90% of the cells were viable after incubation with the nanoprobe for 24 hours, indicating that the $SGNR_1$-SYL3C nanoprobe is biocompatible to the cells.

Photothermal Effect of the SGNR and the LGNR Based SYL3C Nanoprobes

The size-dependent photothermal effect of the GNRs-SYL3C nanoprobes was investigated by comparing FLO-1 cells and the HEK293 cells treated with $SGNR_1$-SYL3C and LGNR-SYL3C nanoprobes against their two controls (cell treated with GNR-MHA and cell only). Figure 7 depicts the optical images of the FLO-1 and the HEK293 cell samples after illumination at the surface plasmon resonance wavelength of the nanoprobes for 1 minute. More blue stained cells were observed on the nanoprobes ($SGNR_1$-SYL3C and LGNR-SYL3C) treated FLO-1 cells than that found in HEK293 cells (Figure 7c, e & Figure 7g, j), indicating more cell death in FLO-1 cells in comparison to HEK293. In addition, more FLO-1 cells died with $SGNR_1$-SYL3C treatment than that with LGNR-SYL3C nanoprobe (Figure 7c &.7e). This is not surprising as we have demonstrated previously that the SGNRs have enhanced photothermal effect than the LGNRs in a mimic

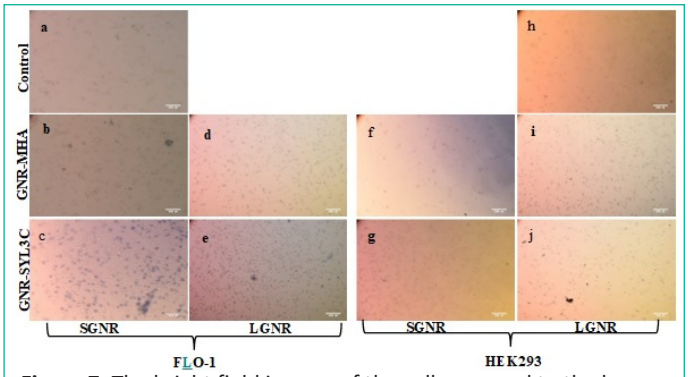

Figure 7: The bright field images of the cells exposed to the laser for 1 minute; FLO-1 cell (a) control; treated with (b) $SGNR_1$-MHA; (c) $SGNR_1$-SYL3C nanoprobe; (d) LGNR-MHA and (e) LGNR-SYL3C nanoprobe; HEK293 cell treated with (f) $SGNR_1$-MHA (g) $SGNR_1$-SYL3C nanoprobe; (i) LGNR-MHA; (j) LGNR-SYL3C nanoprobe and (h) cell control.

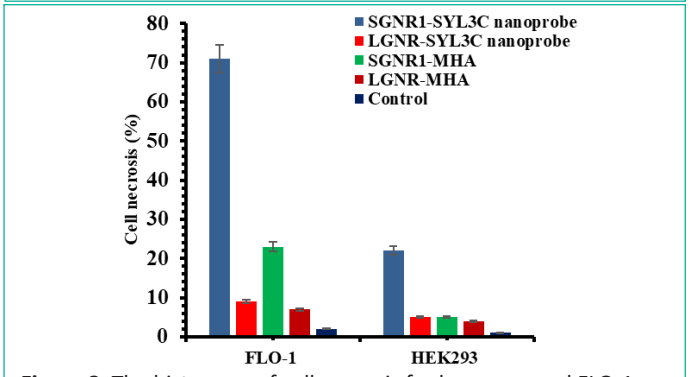

Figure 8: The histogram of cell necrosis for laser exposed FLO-1 and HEK293.

cellular matrix [10]. In comparison to the nanoprobes treated cells, the GNRs-MHA treated FLO-1 and HEK293 cells (Figure7b, d, f, i) and cell only samples (Figure 7a, h) displayed less blue stained cells, indicating fewer dead cells caused by laser irradiation. No significant difference was found for the FLO-1 cells treated with the $SGNR_1$-MHA and the LGNR-MHA respectively.

To compare the photothermal effect of LGNR and SGNR, the cell necrosis due to LGNRs was calibrated by a factor of 1.13 taking into account the slightly higher laser power density used in $SGNR_1$ study. The bar chart of cell necrosis for laser treated cell samples, Figure 8, shows that $SGNR_1$-SYL3C treated FLO-1 and LGNR-SYL3C treated FLO-1 have 71% and 9% dead cells respectively, higher than 23% and 7% from FLO-1 cells treated with $SGNR_1$-MHA and LGNR-MHA, while the control, FLO-1 cell sample had only 2% dead cells. In addition, HEK293 cells treated with the $SGNR_1$-SYL3C and the LGNR-SYL3C nanoprobes have 22% and 5% dead cells, respectively, comparable to 5% and 4% from HEK293 cells treated with $SGNR_1$-MHA and LGNR-MHA, as well as 1% from control HEK293 cells. Thus, it is evident that GNRs-SYL3C nanoprobes treatment induced more cell death in FLO-1cells than GNRs-MHA (without SYL3C) treatment and control cells after laser irradiation. Significantly, the $SGNR_1$-SYL3C nanoprobe induced more than twice dead cells in comparison to the cell line treated with the same GNRs without aptamer functionalization and more than 13 times in comparison to the cell line without GNRs. In addition, FLO-1 cells treated with the $SGNR_1$-SYL3C have more cell death than HEK293 cells. This is consistent with the findings in the fluorescence microscopy and flow cytometry study, which showed that GNRs-SYL3C nanoprobes have a higher binding affinity and specificity for the EpCAM over-expressed cancer cells [23,43,44] than GNRs-MHA [31], highlighting the benefit of targeted nanoprobes in

the photothermal therapy of cancer. Moreover, the FLO-1 cells treated with the $SGNR_1$-SYL3C nanoprobe died 7x more in comparison to the same cells treated with the LGNR-SYL3C nanoprobe. Similarly, $SGNR_1$-MHA introduced more cell death in FLO-1 cells under laser irradiation than LGNR-MHA. This is in line with previous finding that SGNRs generate more heat than LGNRs in cell-mimic environment [10].

Conclusion

This study has successfully synthesized SGNR-SYL3C nanoprobes for targeted photothermal therapy of EpCAM expressed cancer cells. The SGNR-SYL3C nanoprobes showed low toxicity on both cancer and non-cancer cells, The SGNR-SYL3C nanoprobes have a higher affinity to cancer cells with EpCAM overexpression than a normal kidney cell line, HEK293. Furthermore the SGNR-SYL3C nanoprobes exhibited specific binding to the membrane of FLO-1 and MCF-7 cells with high level of EpCAM expression. After laser irradiation, the GNR-SYL3C nanoprobes induced a higher death rate in FLO-1 cells than the same GNRs without targeting ligand, with the death rate being significantly higher in FLO-1 than that in HEK293 cells. Moreover, the death rate of FLO-1 cells treated with SGNR-nanoprobes was higher than those treated with the LGNR-nanoprobes. These demonstrate an enhanced efficacy of SGNR-SYL3C nanoprobes in the photothermal therapy resulting from an increased affinity to EpCAM expressed cancer cells and the enhanced photothermal effect of the SGNRs. These findings provide valuable insight into the development of gold nanoprobes with superior photothermal effect for efficient photothermal therapy of cancer.

Author Statements

Acknowledgments

The authors acknowledge financial support from BBSRC (BB/S018700/1). Zendesha Stepehen Mbalaha acknowledges a PhD studentship from Joseph Sarwuan Tarka University, Makurdi and a grant from the Rank Prize Fund.

Supporting Information

Lists of reagents used for preparing LGNRs and SGNRs, UV-vis extinction spectra and enlarged bright field images of FLO-1 and HEK293 cells after exposure to the laser.

References

1. Khan NU, Lin J, Younas MR, Liu X, Shen L. Synthesis of gold nanorods and their performance in the field of cancer cell imaging and photothermal therapy. Cancer Nano. 2021; 12: 20.

2. Adelt M, MacLaren DA, Birch DJS, Chen Y. Morphological changes of silica shells deposited on gold nanorods: implications for nanoscale photocatalysts. ACS Applied Nano Materials. 2021; 4: 7730-7738.

3. Patibandla S, Zhang Y, Mohammad A, Gu P, Reilly J, Chen Y, et al. Comparative analysis of the toxicity of gold nanoparticles in zebrafish. J Appl Toxicol. 2018; 38: 1153-1161.

4. Chen Y, Zhang Y, Birch DJS, Barnard AS. Creation and luminesceince of size-selected gold nanorods. Nanoscale. 2021; 4: 5017-5022.

5. Zhang Y, Wei G, Yu J, Birch DJS, Chen Y. Surface plasmon enhanced energy transfer between gold nanorods and fluorophores: application to endocytosis study and RNA detection. Faraday Discussion. 2015; 178: 383-394.

6. An L, Wang Y, Tian Q, Yang S. Small gold nanorods: recent advances in synthesis, biological imaging, and cancer therapy. Materials. 2017; 10: 1372-1392.15.

7. Liu Y, Bhattarai P, Dai Z, Chen X. Photothermal therapy and photoacoustic imaging via nanoteranostics in fighting cancer. Chem Soc Rev. 2019; 48: 2053-2108.

8. Singh P, Pandit S, Mokkapati VRSS, Garg A, Ravikumar V, Mijakovic I. Gold nanoparticles in diagnostics and therapeutics for human cancer. International journal of molecular sciences. 2018; 19: 1979-1995.

9. Mbalaha ZS. Gold Nanorod based Nanoprobes for Biomedical Applications. PhD thesis, University of Strathclyde. 2020.

10. Mbalaha ZS, Birch DJS, Chen Y. Photothermal effects of gold nanorods in aqueous solution and gel media: Influence of particle size and excitation wavelength. IET nanobiotechnology. 2023; 17: 103-111.

11. Shamaila S, Zafar N, Riaz S, Sharif R, Nazir J, Naseem S. Gold nanoparticles: an efficient antimicrobial agent against enteric bacterial human pathogen Nanomaterials. 2016; 6: 71-80.

12. Warrier P, Yuan, Y, Beck MP, Teja AS. Heat transfer in nanoparticle suspensions: modeling the thermal conductivity of nanofluids. AIChE Journal. 2010; 56: 3243-3256.

13. Jia H, Fang C, Zhu XM, Ruan Q, Wang YXJ, Wang J. Synthesis of absorption-dominant small gold nanorods and their plasmonic properties. Langmuir. 2015; 31: 7418-7426.

14. Song Y, Zhu Z, An Y, Zhang W, Zhang H, Liu D, et al. Selection of DNA aptamers against epithelial cell adhesion molecule for cancer cell imaging and circulating tumor cell capture. Anal Chem. 2013; 85: 4141-4149.

15. Manivasagan P, Hoang G, Moorthy MS, Mondal S, Doan VHM, Kim H, et al. Chitosan/fucoidan multilayer coating of gold nanorods as highly efficient near infrared photothermal agents for cancer therapy. Carbohydrate Polymers. 2019; 211: 360-369.

16. Bucharskaya AB, Maslyakova GN, Chekhonatskaya ML, Terentyuk GS, Navolokin NA, Khlebtsov BN, et al. Plasmonic photothermal therapy: approaches to advanced strategy. Lasers in Surgery and Medicine. 2018; 50: 1025-1033.

17. Vu DT, Vu-Le TT, Nguyen VN, Le QM, Wang CRC, Chau LK, e al. Gold nanorods conjugated upconversion nanoparticles nanocomposites for simultaneous bioimaging, local temperature sensing and photothermal therapy of OML-1 oral cancer cells. International Journal of Smart and Nano Materials. 2021; 12: 49-71.

18. Awan UA, Raza A, Ali S, Saeed RF, Akhtar N. Doxorubicin-loaded gold nanorods: a multifunctional chemo-photothermal nanoplatform for cancer management. Beilstein J Nanotechnol. 2021; 12: 295-303.

19. Li Z, Huang H, Tang S, Li Y, Yu X, Wang H, et al. Small gold nanorods laden macrophages for enhanced tumor coverage in photothermal therapy, Biomaterials. 2016; 74: 144-154.

20. Yang H, Chen Z, Zhang L, Yung WY, Leung KCF, Chan HYE, et al. Mechanism for the cellular uptake of targeted gold nanorods of defined aspect ratios. Small. 2016; 12: 5178-5189.

21. Gupta N, Malviya R. Understanding and advancement in gold nanoparticle targeted photothermal therapy of cancer. BBA – reviews on Cancer. 2021; 1875: 188532.

22. Wang N, Liu H, Hao J, Bai X, Li H, Zhang Z, et al. Single molecular recognition force spectroscopy study of a DNA aptamer with the target epithelial cell adhesion molecule. Analyst. 2015; 140: 6226-6229.

23. Song Y, Zhu Z, An Y, Zhang W, Zhang H, Liu D, et al. Selection of DNA aptamers against epithelial cell adhesion molecule for cancer cell imaging and circulating tumor cell capture. Anal Chem. 2013; 85: 4141-4149.

24. Minhee K, Kim D, Kim K, Jung W, Kim D. Applications of cancer cell-specific aptamers in targeted delivery of anticancer therapeutic agents. Molecules. 2018; 23: 830-849.

25. Amaya-Gonzalez S, Ide-los-Santos-Alvarez N, Miranda-Ordieres AJ, Lobo-Castanon MJ. Aptamer-based analysis: a promising alternativefor food safety control. Sensors. 2013; 13: 16292-16311.

26. Wang Y, Li J, Qiao P, Jing L, Song Y, Zhang J, et al. Screening and application of a new aptamer for the rapid detection of Sudan dye lll. European Journal of Lipid Science and Technology. 2018; 120: 1700112-1700118.

27. Pu Y, Liu Z, Lu Y, Yuan P, Liu J, Yu B, et al. Using DNA aptamer probe for immunostaining of cancer frozen tissues. Analytical Chemistry. 2015; 87: 1919-1924.

28. Munz M, Baeuerle PA, Gires O. The emerging role of EpCAM in cancer and stem cell signaling. Cancer Res. 2009; 69: 5627-5629.

29. Zheng T, Zhang Q, Feng S, Zhu JJ, Wang Q, Wang H. Robust nonenzymatic hybrid nanoelectrocatalysts for signal amplification toward ultrasensitive electrochemical cytosensing. Journal of the American Chemical Society. 2014; 136: 2288-2291.

30. Garcia E, Hayden A, Birts C, Britton E, Cowie A, Pickard K, et al. Authentication and characterisation of a new oesophageal adenocarcinoma cell line: MFD-1. Scientific Reports. 2016; 6: 32417-32429.

31. Chen Y, Cheng B, He Z, Wang S, Wang Z, Sun M, et al. Capture and identification of heterogeneous circulating tumor cells using transparent nanomaterials and quantum dots-based multiplexed imaging. Journal of Cancer. 2016; 7: 69-79.

32. Liu Z, Lu Y, Pu Y, Liu J, Liu B, Yu B, et al. Using aptamers to elucidate esophageal cancer clinical samples. Science Reports. 2015; 5: 18516-18524.

33. Lai X, Zou Y, Wang S, Zheng M, Hu X, Liang HY, et al. Modulating the morphology of gold graphitic nanocapsules for plasmon resonance-enhanced multimodal imaging. Anal Chem. 2016; 88: 5385−5391.

34. Song Y, Shi Y, Huang M, Wang W, Wang Y, Cheng J, et al. Bioinspired engineering of a multivalent aptamer-functionalized nanointerface to enhance the capture and release of circulating tumor cells. Angew Chem Int Ed. 2019; 58: 2236-2240.

35. Wei G, Yu J, Wang J, Gu P, Birch DJS, Chen Y. Hairpin DNA-functionalized gold nanorods for mRNA detection in homogenous solution. Journal of Biomedical Optics. 2016; 21: 097001-097009.

36. Mbalaha ZS, Edwards PR, Birch DJS, Chen Y. Synthesis of small gold nanorods and their subsequent functionalization with hairpin single stranded DNA. ACS Omega. 2019; 4: 13740-13746.

37. Wijaya A, Hamad-Schifferli K. Ligand customization and DNA functionalization of gold nanorods via round-trip phase transfer ligand exchange. Langmuir. 2008; 24: 9966-9969.

38. Zhong J, Ding J, Deng L, Xiang Y, Liu D, Zhang Y, et al. Selection of DNA Aptamers Recognizing EpCAM-Positive Prostate Cancer by Cell-SELEX for in vitro and in vivo MR Imaging. Drug Design Development and Therapy. 2021; 15: 3985–3996.

39. Gires O, Puhr M. EpCAM is overexpressed in local and metastatic prostate cancer, suppressed by chemotherapy and modulated by MET-associated miRNA-200c/205. Br J Cancer. 2014; 111: 955-964.

40. Ni J, Cozzi P, Beretov J, Duan W, Bucci J, Graham P, et al. Epithelial cell adhesion molecule (EpCAM) is involved in prostate cancer chemotherapy/radiotherapy response in vivo. BMC Cancer. 2018; 18: 1092-1104.

41. de Wit S, Manicone M, Rossi E, Lampignano R, Yang L, Zill B, et al. EpCAM(high) and EpCAM(low) circulating tumor cells in metastatic prostate and breast cancer patients. Oncotarget. 2018; 9: 35705-35716.

42. Tretter JY, Schorpp K, Luxenburger E, Trambauer J, Steiner H, Hadian XK, et al. A high-content screen for small-molecule regulators of epithelial cell-adhesion molecule (EpCAM) cleavage yields a robust inhibitor. J Biol Chem. 2018; 293: 8994-9005.

43. Wang J, Zhu G, You M, Song E, Shukoor MI, Zhang K, et al. Assembly of aptamer switch probes and photosensitizer on gold nanorods for targeted photothermal and photodynamic cancer therapy. ACS Nano. 2012; 6: 5070-5077.

44. Li Z, Tang S, Wang B, Li Y, Huang H, Wang H, et al. Metabolizable small gold nanorods: size-dependent cytotoxicity, cell uptake and in vivo biodistribution. ACS Biomaterials Science & Engineering. 2016; 2: 789-797.